RSC Advances

ROYAL SOCIETY OF CHEMISTRY

www.rsc.org/advances

RSC Advances

RSCPublishing

ARTICLE

Synthesis of novel micro/mesoporous composite material Beta-FDU-12 and its hydro-upgrading performance for FCC gasoline

Peng Du[1], Peng Zheng[1], Shaotong Song[1], Xilong Wang[1], Minghui Zhang[1], Kebin Chi[2], Chunming Xu[1], Aijun Duan[1,*], Zhen Zhao[1,*]

Cite this: DOI: 10.1039/x0xx00000x

Received 00th January 2012,
Accepted 00th January 2012

DOI: 10.1039/x0xx00000x

www.rsc.org/

A novel micro/mesoporous composite material Beta-FDU-12 (BF) was successfully synthesized via a nano-assembling method. BF was used as the catalyst support additive that mixed with γ-Al_2O_3, when preparing the hydro-upgrading catalyst. The BF micro/mesoporous material and its corresponding catalyst CoMo/BFA were characterized using SAXS, XRD, FTIR, TEM, N_2 adsorption-desorption, Pyridine-FTIR, UV-Vis DRS, Raman and XPS techniques. The physicochemical properties of CoMo/BFA were compared to those of the reference catalysts with different support materials including γ-Al_2O_3, FDU-12-γ-Al_2O_3 and ZrFDU-12-γ-Al_2O_3. The characterization results demonstrated that CoMo/BFA showed excellent textural and acidic properties. Furthermore, the addition of EDTA by the post-treatment method improved the dispersion of the active metals. The catalyst CoMoE/BFA exhibited the best hydro-upgrading performance of FCC gasoline (HDS efficiency 94.2 % and RON loss 0.8 unit), which could be attributed to the synergistic effects of the open porous structure, excellent textural property, appropriate acidity, and the favorable dispersivity of the active centers.

1. Introduction

Environmental protection is one of the most prominent issues concerning the public along with the economic development of the world. The current challenge is the exhaust emission control of transportation fuels, thus, the sulfur content in gasoline must be reduced to a very low level to meet the specification of ultra clean fuel. Hydro-upgrading is currently one of the most widely used techniques in the petroleum refining industry. However, the gasoline octane number will suffer a large decrease due to olefin saturation in the hydrogenation process. Therefore, the design and development of novel catalysts which can not only focus on the desulfurization performance but also on the preservation of the octane number are very important in improving the hydroprocessing technology.

The supported catalyst is still one of the most important kinds of hydro-upgrading catalysts. However, due to their deficiencies of the single Lewis acid sites distribution and amorphous pore structures, the conventional industrial alumina-supported CoMo catalysts cannot meet the requirement of the ultra-deep desulfurization. These catalysts also show a strong interaction with the active metals, which inevitably inhibits the HDS activity[1]. As a consequence, many researchers began to explore some novel catalysts through different methods, such as improving the metal dispersion[2], or using additives[3] and adopting new supports, i.e., ordered mesoporous silica-aluminas[4] and mesoporous silica molecular sieves[5,6].

In recent years, zeolites which possess the advantages of strong acidity, high stability, shape selectivity and moderate metal support interactions have attracted extensive attentions. Zeolite Beta showed tunable and suitable acidity, higher hydroisomer-ization activity, lower hydrogen-transfer capacity and lower catalyst deactivation[7,8]. The research of Mobile company[9-11] reported that the catalysts containing Beta had distinct advantages in increasing the efficiency of desulphurization, maintaining the gasoline octane number and

[1] State Key Laboratory of Heavy Oil Processing, China University of Petroleum, Beijing 102249, P. R. China;
[2] Petrochemical Research Institute, PetroChina Company Limited, Beijing 100195, P. R. China;
*Aijun Duan: duanaijun@cup.edu.cn ; Zhen Zhao: zhenzhao@cup.edu.cn

lowering the hydrogen consumption, compared with the hydro-upgrading catalyst containing ZSM-5 with FCC light gasoline as feedstock. However, its small pores limited its application in some processes involving large reactant molecules.

The large pore sizes and high specific surface areas of mesoporous materials can compensate for the diffusion disadvantages of microporous zeolites. Admittedly, the unidirectional pore systems in the two-dimensional (2D) mesostructures cause more diffusion resistance than the pore systems in three-dimensional (3D) mesostructure with the same pore size. FDU-12 is a type of three-dimensional (3D) mesoporous material with face-centred cubic (Fm3m) structure[12]. Compared with other mesoporous materials, FDU-12 possesses a higher specific surface area (800~1000 $m^2 \cdot g^{-1}$) and a wider range of aperture (4~27 nm), indicating that FDU-12 are more favorable for the dispersion of active sites and the diffusion of guest molecules. Nevertheless, these pure silicon mesoporous materials exhibit weak acidity in the catalysis reactions, which is detrimental to their catalytic performances. In order to modify the acidity of the pure silicon material, some heteroatoms (such as Al, Ti and Zr) were introduced to prepare metal modified mesoporous materials. For example, Salas[13] successfully synthesized ordered Zr-modified MCM-41 molecular sieves via a surfactant-templated method, the obtained results showed that strong Brønsted acidity can be formed on the solid. These Zr-modified mesoporous materials with ordered pore system and surface acidity have been investigated extensively to be used as the supports of HDS catalysts[14-16]. Another common method to introduce acid sites to the pure silicous materials is to incorporate different microporous zeolites with high B acidity. Thus, the composites of micro-mesoporous zeolites containing both types of porosity have been developed. This new material primarily combines the advantages of microporous and mesoporous materials. Many kinds of micro-mesoporous materials like Y-MCM-41[17], ZSM-5/KIT-6[18], and Beta-KIT-6[19], had already been synthesized and applied in the field of catalysis. Materials with multiple acidity as well as good diffusivity can significantly improve the HDS catalytic activity.

Another key point in preparing highly active catalysts is to improve the dispersion degree of the active metals. The addition of chelating agents can not only improve the catalyst activity and stability, but also balance the interaction between metal and support[20]. Many kinds of chelating ligands such as nitrilotriacetic acid (NTA), cyclohexanediamine-tetraaceticacid (CyDTA), citric acid (CA), and ethylene diamine tetraacetic acid (EDTA) have been used in the preparation of hydrotreating catalysts and showed positive effects[21-23]. Among these, EDTA was one of the most widely studied chelating ligands. Pena et al.[24] used EDTA as the chelating agent for preparing CoMo/SBA-15 catalysts and applied in HDS of dibenzo-thiophene. And they found that the catalysts prepared with EDTA displayed high HDS performance. This is because the addition of EDTA significantly increased the dispersion of metal species.

In this work, a novel micro/mesoporous composite material Beta-FDU-12 (BF) was successfully synthesized from zeolite Beta seeds using a nano-assembling method. Beta-FDU-12 possesses both large pore (larger than 10 nm) and the three-dimensional (3D) mesostructure which can further enhance mass transfer. Furthermore, Beta-FDU-12 possesses Beta microporous structure and cubic Fm3m mesoporous structure of FDU-12 simultaneously. The acidity of Beta-FDU-12 is similar to Beta zeolite and higher than that of the FDU-12 mesoporous material. The superior mass transfer property and the appropriate acidity make Beta-FDU-12 composites more suitable for the HDS of FCC gasoline. In addition, until now, the synthesis and catalytic application of Beta-FDU-12 have, to our best knowledge, not been reported. Considering the cost of the overall catalysts and the defects of alumina together, the obtained BF composite materials were used as the support additives of alumina support when applied in the HDS reaction. Meanwhile, the other support additives, FDU-12 and ZrFDU-12 were also prepared to well compare the HDS activity of gasoline. Furthermore, EDTA was added by a post-treatment method to improve the active metal dispersion on the catalyst CoMo/BF-γ-Al_2O_3 and to moderate the interaction between the active metal and the support. The correlations between the hydro-upgrading performances of FCC gasoline and the corresponding catalysts were discussed.

2. Experimental

2.1 Synthesis of materials

The micro/mesoporous composite material Beta-FDU-12 (BF) was hydrothermally synthesized from the in-situ assembly of $EO_{106}PO_{70}EO_{106}$ (Pluronic F127, Aldrich) with a preformed Beta microcrystal solution. Firstly, zeolite Beta microcrystal solution was prepared with the molar ratio of 100 SiO_2: 1.0 Al_2O_3: 1.4 Na_2O: 15 TEAOH: 360 H_2O. Specific steps were as follows: 0.19 g of NaOH, 0.23 g of $NaAlO_2$ and 21.43 g of tetraethylorthosilicate (TEOS) were added into 25.95 g of an aqueous TEAOH solution (25 wt%). Then, the mixture was stirred for 2-4 h at room temperature and heated at 413 K in a Teflon-lined autoclave for 24 h. The zeolite Beta seed solution was obtained as the precursor. Secondly, 2.0 g of triblock copolymers F127, 5.00 g of KCl and 2.0 g of 1,3,5-trimethylbenzene (TMB) were dissolved in 120ml of 2.0 M HCl aqueous solution with stirring at low temperature 288 K for 24 h. Then 8.3 g of tetraethylorthosilicate (TEOS) as the silicate source was added dropwise into the above surfactant solution for 2 h. Afterwards the zeolite Beta seed solution precursor was added to the above solution with vigorous stirring for another 24 h. It is worth noting that the entire stirring process was carried out at a low temperature of 288 K. Finally, the mixture was transferred into a Teflon bottle and heated statically at 373 K for 48 h. The final as-synthesized product was obtained by filtering, washing with distilled water, and drying at 353 K for 24 h in air, and ultimately, calcined at 823K for 6 h.

ZrFDU-12 with Si/Zr = 20 was synthesized using a direct synthesis method reported in the literature[20]. Typically, 2.0 g of F127, 2.0 g of TMB and 5.0 g of KCl were dissolved in 120 mL of 1.5 M HCl and stirred at 288 K for 24 h. 8.3 g of TEOS was added. After three hours, 0.64 g of $ZrOCl_2 \cdot 8H_2O$ was added into the resulting reaction mixture, which was stirred for a further 24 h at the same temperature then transferred to an autoclave and heated at 373K for 48 h. The solid was isolated by filtration with deionized water and dried at 353 K for 6 h. The resulting silica surfactant composite powder was calcined at 823 K for 6 h to obtain the composite, denoted as ZrFDU-12 sample.

Beta zeolite was prepared in the same way as the zeolite seeds described in the BF synthesis. Specific steps were as follows: 0.19 g of NaOH, 0.23 g of $NaAlO_2$ and 21.43 g of tetraethylorthosilicate (TEOS) were added into 25.95 g of an aqueous TEAOH solution (25 %). Then, the mixture was stirred for 2-4 h at room temperature and heated at 413 K in a Teflon-lined autoclave for 48 h. The aluminosilicate precursor was collected by filtration, dried at 373 K for 10 h, and calcined at 823 K in air for 6 h to remove the templates.

FDU-12 was prepared by a low-temperature strategy as described in the literature[25].

2.2 Preparation of catalysts

H-type materials of Beta-FDU-12(BF) were obtained by ion-exchanged with a 1.0 M NH_4Cl aqueous solution at 353 K for 2 h. Then filtered and calcined at 823 K in air for 6 h. Different supports (FDU-12, ZrFDU-12 and BF) were prepared by the extrusion method using the above materials as additives covering 20 wt% in support and the residue is 80 wt% pseudo-boehmite (Aluminum Corporation of China Limited, 69.5 wt%) acting as the binder. All the catalysts were prepared following the two-step incipient-wetness impregnation procedures. 10 wt % of MoO_3 and 5 wt% of CoO were impregnated on the above support material with ammonium molybdate solution and cobalt nitrate solution, respectively. The sample was dried at 373 K for 6 h and calcined at 823 K for 5 h to obtain the catalysts. To prepare the catalyst with EDTA, CoMo/BF-γ-Al_2O_3 was impregnated with EDTA solution by the post-treatment method. An appropriate amount of ammonium hydroxide was added to speed up the dissolution of EDTA. The mixture was dried at 373 K for 6 h to obtain the catalyst CoMo-EDTA/BF-γ-Al_2O_3. The calcination of this material was not carried out in order to prevent the decomposition of the chelating agent in the catalyst precursors. Then the obtained samples were crushed into 0.3-0.5 mm particles for the later use. The resulting catalysts were denoted as CoMo/γ-A (CoMo/γ-Al_2O_3), CoMo/FA (CoMo/FDU-12-γ-Al_2O_3), CoMo/ZFA (CoMo/ZrFDU-12-γ-Al_2O_3), CoMo/BFA (CoMo/BF-γ-Al_2O_3) and CoMoE/BFA (CoMo-EDTA/BF-γ-Al_2O_3), respectively.

2.3 Characterization of the supports and catalysts

Small-angle X-ray scattering (SAXS) patterns were recorded on a NanoSTAR Small-Angle X-ray scattering system (Bruker, Germany) using Cu Kα radiation (40 kV, 35 mA).

X-ray powder diffraction (XRD) patterns of the samples were recorded with a Shimadzu X-6000 diffraction Cu Kα radiation. The 2θ range was from 5^o to 80^o and the diffractometer was operated at 30 mA.

Fourier transform infrared spectroscopy (FTIR) absorbance spectra were performed on a FTS-3000 spectrophotometer with wave numbers ranging from 4000 to 400 cm^{-1}. The transparent discs were prepared using 2 mg of the samples mixed with 200 mg of dry KBr.

Nitrogen sorption isotherms of the samples were obtained by a Micromeritics TriStar II 2020 porosimetry analyzer at -77 K. The specific surface areas of the samples were calculated using the Brunauer-Emmett-Teller (BET) method. The total volumes of micro- and mesopores were calculated from the amounts of nitrogen adsorbed at p/p_o = 0.98. The pore size distribution (PSD) was derived from the desorption branches of the isotherms using the Barrett-Joyner-Halenda (BJH) method.

Transmission electron microscopy (TEM) images were performed with a JEOL JEM 2100 electron microscope operated at an accelerating voltage of 200 kV. The samples were milled in an agate mortar and then ultrasonically suspended in ethanol. A drop of the supernatant liquid was placed on a copper grid coated with a sputtered carbon polymer.

Surface acid amounts and types of the samples were analyzed by a pyridine-FTIR (Py-FTIR) spectroscopy on a MAGNAIR 560 FTIR instrument with a resolution of 1 cm^{-1}. The samples were dehydrated at 873 K for 5 h under a vacuum of 1.33×10^{-3} Pa, followed by adsorption of purified pyridine vapor at room temperature for 20 min. The system was then degassed and evacuated at different temperatures, and the IR spectra were recorded.

The UV-Vis diffuse reflectance spectroscopy (UV-Vis DRS) was recorded in the wavelength range of 200-800 nm using a UV-Vis spectrophotometer (Hitachi U-4100) equipped with the integration sphere diffuse reflectance attachment. The powder catalysts were loaded in a transparent quartz and a pure $BaSO_4$ support was used as a reference.

Raman spectra were recorded on a Renishaw Micro-Raman System 2000 spectrometer with spectral resolution of 2 cm^{-1}. The 325 nm line from a He/Cd laser was used as the exciting source with an output of 20 mW. The Raman spectra between 200 cm^{-1} and 1200 cm^{-1} were automatically recorded at room temperature by the condition of 50 s accumulation at a 1 cm^{-1} resolution.

X-ray photoelectron spectroscopy (XPS) analyses of the sulfided catalysts were carried out in a Thermo Fisher K-Alpha spectrometer equipped with an analyser mode of CAE operating at a fixed pass energy of 40 eV and working under vacuum ($<10^{-9}$ mbar). All the data were acquired using Kα (hv = 1486.6 eV), and the binding energy were calibrated taking C 1s (BE = 284.6 eV) as an internal standard. Before analysis, the catalysts were freshly presulfided according to the same

sulfidation procedure as the catalytic activity evaluation, and stored under cyclohexane to prevent oxidation.

2.4 Catalytic performance evaluation

Two grams of catalysts were used to evaluate the HDS activity of FCC gasoline in a fixed-bed inconel reactor. Prior to the catalytic activity evaluation, the catalysts were sulfided at 320°C for 4 h in a stream of 2 wt% CS_2-cyclohexane in H_2 under a pressure of 2.5 MPa. After the presulfurization step, the catalysts were evaluated at 270 °C, with a pressure of 2.0 MPa, H_2/Oil ratio of 300 mL/mL and WHSV of 2.0 h^{-1}. The sulfur contents were analyzed by a RPP-2000SN sulfur & nitrogen analyzer (Taizhou Central Analytical Instruments Co. Ltd. P.R. China). To corroborate the product identification, including group composition and octane number of gasoline, the product mixture was measured using gas chromatography and analyzed by the GC99 calculation software which was developed by Beijing Petroleum Science Research Institute.

The catalytic activity was estimated by the HDS efficiency (HDS %) which was defined as follows:

$$HDS\ \% = [(S_f - S_p)/S_f] \times 100\%$$

where S_f and S_p are the sulfur concentrations in the feed and product respectively.

3. Results and discussion

3.1 Characterization of the supports and catalysts

3.1.1 SAXS characterization

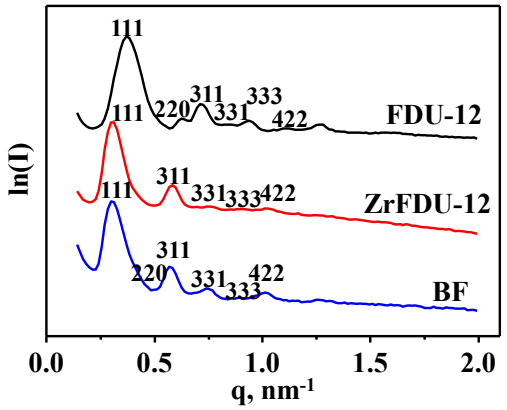

Fig. 1. SAXS traces of the as-synthesized materials.

The small-angle X-ray scattering patterns of FDU-12, ZrFDU-12 and BF are shown in Fig. 1. The FDU-12 sample exhibits six scattering peaks, which can be exactly indexed to the (111), (220), (311), (331), (333) and (442) reflections of a face-centered cubic structure (Fm3m)[25], indicating that the mesoporous silica FDU-12 was synthesized successfully.

As shown in Fig. 1, the typical face-centered cubic (fcc) mesostructure is maintained for the ZrFDU-12 samples. However, compared with the pure FDU-12 sample, the intensities of the diffraction peaks decrease to some extent, reflecting a less ordered fcc mesoporous structure in the ZrFDU-12 sample. This may be caused by the incorporation of Zr species into the mesoporous channels resulting in the configuration disorders. A typical SAXS pattern of the BF sample also exhibits six peaks similar to the FDU-12 sample, which implys that the micro/mesoporous material BF possesses a similar structure to the fcc mesoporous silica.

3.1.2 TEM characterization

Transmission electron microscopy (TEM) images confirms large ordered porosity domains for the pure FDU-12 material (in Fig. 2). The views recorded along the (111) and (100) crystallographic directions agree well with the cubic Fm3m symmetry for FDU-12. Meanwhile, the TEM images of BF (in Fig. 2) show the same mesoporous channels as FDU-12, which confirm that both FDU-12 and BF possess the well-ordered cubic Fm3m mesostructure. It is also noticed that all the ZrFDU-12 materials with Si/Zr ratio = 20 have similar mesostructures but less order due to the incorporation of zirconium ions into the framework. The large pores (~20 nm) are clearly visible in the TEM images. These observations are consistent with the results obtained from N_2 adsorption.

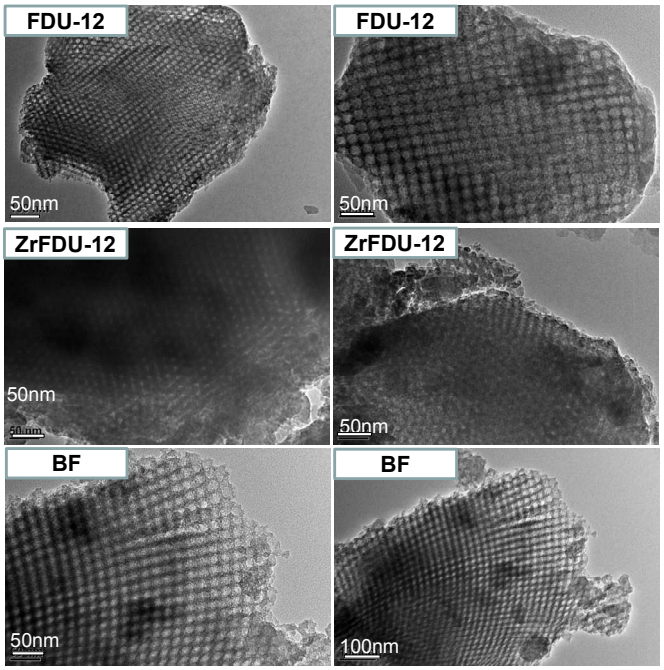

Fig. 2. TEM images of the as-synthesized materials.

3.1.3 FTIR spectroscopy

The skeleton information of the as-synthesized materials was analyzed by means of FTIR (see Supporting Information, Fig. S1). For all the samples, the adsorption peaks at 460 cm^{-1}, 805 cm^{-1} and 1025 cm^{-1} are attributed to the stretching vibrations of Si-O-Si bands. While for the ZrFDU-12 sample, the band at 950 cm^{-1} is caused by the surface silanol group. Compared with the pure FDU-12 sample, absorption peak at 805 cm^{-1}, the Si-O-Si symmetric stretching vibration frequencies of the ZrFDU-

12 sample have a red shift to 820 cm^{-1}, which reveals that the coordination interactions may have taken place. Moreover, it can be seen from the spectra of the ZrFDU-12 sample that there is a shoulder peak at 960 cm^{-1}. According to the Ref.[26], this shoulder peak is due to asymmetry of the framework because of the existence of defects. A strong shoulder peak means a decrease of the framework symmetry. These can be taken as proof for the tetrahedrally coordinated zirconium species incorporated into the silica framework. Also, it can be seen from Fig. S1 that the BF composite material has a specific absorption peak similar to that of FDU-12. Furthermore, the bands at 520 cm^{-1} and 570 cm^{-1} are assigned to the vibrations of five- and six-membered rings, respectively, which indicates that the BF composite material has both the skeleton structure of FDU-12 and Beta[27].

3.1.4 Porous properties of the materials and catalysts

Table 1. Textural properties of the supports and corresponding CoMo catalysts

Catalyst Number	S_{BET}[a] ($m^2 \cdot g^{-1}$)	V_t[b] ($cm^3 \cdot g^{-1}$)	V_{mes}[c] ($cm^3 \cdot g^{-1}$)	V_{mic}[d] ($cm^3 \cdot g^{-1}$)	Pore Size[e] (nm)
γ-Al_2O_3	191	0.74	0.72	-	14.7
Beta	502	0.34	-	0.22	-
FDU-12	845	0.72	0.71	0.08	17.9
ZrFDU-12	709	0.65	0.63	0.09	18.4
BF	953	0.77	0.69	0.12	17.8
CoMo/γ-Al_2O_3	152	0.54	0.53	0.01	13.3
CoMo/FA	138	0.50	0.49	0.01	13.9
CoMo/ZFA	149	0.51	0.51	0.03	13.7
CoMo/BFA	172	0.48	0.50	0.02	11.9
CoMoE/BFA	145	0.35	0.33	0.01	7.0

Note: [a] Calculated by BET method.

[b] The total pore volume was obtained at a relative pressure of 0.98.

[c] Calculated using BJH method.

[d] Calculated using the t-plot method

[e] Mesopore diameter calculated using the BJH method.

N_2 adsorption-desorption isotherms and pore size distribution curves of different materials are shown in Fig. S2 (see Supporting Information). The materials of FDU-12, ZrFDU-12 and BF exhibit analogous type IV isotherms with H2 type hysteresis loops and narrow mesoporous distributions, which are the characteristics of ordered mesoporous structure. Zeolite Beta displays type I isotherm of microporous material and no mesopores emerge in its pore size distribution curve. Al_2O_3 shows a H4 type hysteresis loop and a broad pore size distribution, which can be ascribed to the interparticle space[28]. From Fig. S3 (see Supporting Information), all the corresponding catalysts show type IV isotherms with H3 type hysteresis loops, since a high proportion of alumina is integrated in the catalysts. The narrow pore size distribution curves are obtained from the isotherms of different catalysts, particularly in CoMoE/BFA.

The textural characteristics of the materials and the corresponding catalysts derived from these N_2 adsorption-desorption isotherms are summarized in Table 1. FDU-12 and ZrFDU-12 show high specific surface areas (845 and 709 $m^2 \cdot g^{-1}$), large pore volumes (0.72 and 0.65 $cm^3 \cdot g^{-1}$) and pore diameters (17.9 and 18.4 nm). BF displays better textural properties than that of zeolite Beta, implying that the introduction of mesoporous surfactants can markedly improve the textual properties of the composite materials. Moreover, the decrease in the textural characteristics of the CoMoE/BFA could be attributed to a little incorporation of chelating agents.

3.1.5 XRD characterization

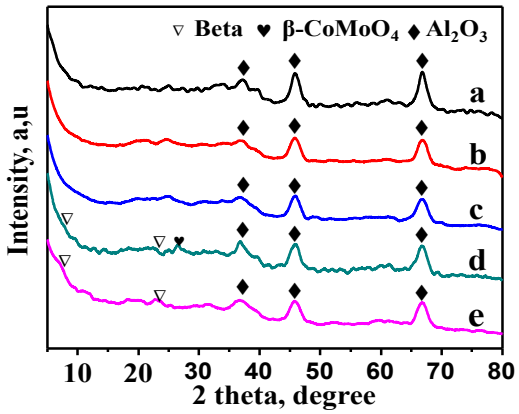

Fig. 3. XRD patterns of the corresponding supported CoMo catalysts. (a) CoMo/γ-Al_2O_3, (b) CoMo/FA, (c) CoMo/ZFA, (d) CoMo/BFA, (e) CoMoE/BFA

Fig. S4 (see Supporting Information) displays the wide-angle XRD patterns of micro-porous zeolite Beta and BF composite material. It can be found that zeolite Beta and BF possess the same characteristic peaks at 2θ = 7.8°, 22.4°, which are the characteristics of zeolite Beta[29]. Compared with pure Beta zeolite, the lower peeks intensities of BF composite material may be due to the formation of a small amount of zeolite Beta nanocrystals with smaller sizes in the first step of the synthesis process. The results combined with SAXS and FTIR characterizations indicate that the as-synthesized material BF is a micro-mesoporous material combining the characteristics of FDU-12 and Beta zeolite.

The wide-angle XRD patterns of different catalysts are shown in Fig. 3. It can be observed that all catalysts have strong signals at 2θ = 36.8°, 46.2° and 66.7°, which are attributed to the characteristic peaks of γ-Al_2O_3. The relatively weak diffraction peaks at 7.8° and 22.4° are indexed as the characteristic peaks of Beta nanocrystals as previously described. The XRD patterns of all catalysts exhibit no obvious MoO_3 diffraction peaks at 2θ = 23.3° and 27.3°, indicating the absence of bulk crystalline MoO_3 on the support.

The CoMo/BFA catalyst, prepared without chelating agents, exhibits the formation of a crystalline phase. This signal at 2θ = 26.5° reveals the formation of the β-$CoMoO_4$ phase which can make an undesirable effect on the catalyst activity[24].

After the addition of chelating agents, the reflection at 26.5° in the CoMo/BFA sample disappears, indicating that the use of chelating agents after the impregnation of the metal species to

the catalyst can inhibit the formation of the β-$CoMoO_4$ crystalline phase, therefore the addition of chelating agents can prevent the agglomeration of Co-Mo species on the catalyst surface.

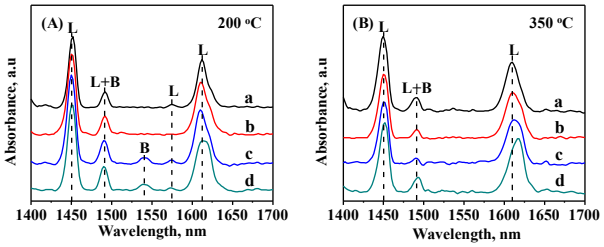

3.1.6 Surface acidity measurement

Fig. 4. FTIR spectra of pyridine adsorbed on (a) CoMo/γ-Al_2O_3, (b) CoMo/FA, (c) CoMo/ZFA, and (d) CoMo/BFA after degassing at (A) 200 °C and (B) 350 °C.

Table 2. Amounts of B and L acid sites determined by FT-IR of pyridine adsorption for different catalysts.

Catalysts Number	200 °C Acid content(μmol·g^{-1})				350 °C Acid content(μmol·g^{-1})			
	L	B	L+B	B/L	L	B	L+B	B/L
CoMo/γ-Al_2O_3	/	66.8	66.8	/	/	49.7	49.7	/
CoMo/FA	/	87.4	87.4	/	/	41.1	41.1	/
CoMo/ZFA	9.1	95.1	104.2	0.096	/	39.4	39.4	/
CoMo/BFA	9.1	92.6	101.7	0.098	/	45.4	45.4	/

The acidities of different catalysts were investigated using the pyridine-FTIR method. Different signals can be observed in the spectra in the region of 1700-1400 cm^{-1} as shown in Fig. 4. According to the literature[30], the bands at 1450 and 1610 cm^{-1} are ascribed to the strong Lewis-bound pyridine, while the band at 1575 cm^{-1} are ascribed to the weak Lewis-bound pyridine, and the bands at 1542 and 1640 cm^{-1} are ascribed to the pyridinium ion ring vibration owing to pyridine molecules bound to Bronsted acid sites. The band at 1492 cm^{-1} was assigned to the pyridine associated with both Brønsted and Lewis sites. The detailed data about the acid strength distribution and the acid quantity of the catalysts are listed in Table 2.

These results (in Table 2) were calculated from the IR spectra collected from the catalysts with pyridine adsorption followed by degassing at 200℃ and 350℃ (the total amounts of acid sites were determined by the pyridine adsorption IR spectra after degassing at 200℃, and the amounts of medium and strong acid sites were determined by the IR pyridine adsorption spectra after degassing at 350℃). After degassing at 200 ℃, the total amounts of acid sites (B + L) of the CoMo/ZFA and CoMo/BFA catalysts are significantly higher than those of the CoMo/γ-Al_2O_3 and CoMo/FA catalysts. Moreover, the acid strength distributions of CoMo/ZFA and CoMo/BFA are almost identical. There is a small amount of weak Brønsted acid sites in CoMo/ZFA and CoMo/BFA due to the presence of the Si-O-Zr species in the ZrFDU-12 sample and H-type zeolite Beta in the BF sample, respectively. The small amount of B acid sites is due to the combination of high percentages of alumina in catalysts. After degassing at 350℃, no Brönsted acid sites are detected in any of the catalysts. The amounts of medium and strong acid sites follow the order:

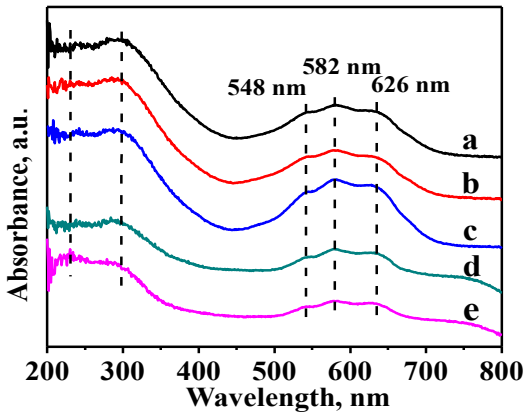

CoMo/γ-Al_2O_3> CoMo/BFA> CoMo/FA> CoMo/ZFA.

3.1.7 UV-vis characterization

Fig. 5. UV-vis DRS spectra of different catalysts. (a) CoMo/γ-Al_2O_3, (b) CoMo/FA, (c) CoMo/ZFA, (d) CoMo/BFA, (e) CoMoE/BFA

The dispersion of Co and Mo oxide species on the catalysts can be analyzed by UV-visible absorption spectroscopy. The UV spectra of different catalysts are shown in Fig. 5. The absorption bands corresponding to ligand-to-metal charge transfer (LMCT) $O^{2-}\rightarrow Mo^{6+}$ can be observed in the 200-360 nm region. The exact position of the bands reflects the local symmetry around the Mo^{6+} depending on their coordination and aggregation states[31].

In these spectra, the absorption band at about 220-250 nm can be observed in all catalysts, but it is well defined in CoMoE/BFA, which indicated an increase in the proportion of dispersed tetrahedral Mo species by the modification due to EDTA. The absorption band at about 250-360 nm proves the existence of the octahedrally coordinated polymolybdate species. The main bands in the visible range locate at 548, 582 and 626 nm. These features have been attributed to the tetrahedral Co (II)[32] incorporated into the alumina as $CoAl_2O_4$. However, the peak intensities are relatively weak in CoMoE/BFA (see Fig. 5e). This phenomena could be interpreted as the presence of Co^{2+} species less polymerized than the reference catalysts.

The UV-DRS characterization results make evidences that the characteristics of the active metals become better dispersed on the surfaces of BF-γ-Al_2O_3 when EDTA is added through the post-treatment method.

3.1.8 Raman characterization

Raman spectra of different catalysts are presented in Fig. 6. For all CoMo catalysts without EDTA, four bands at 325, 845, 930 and 990 cm^{-1} are observed. The bands at 325 cm^{-1} and 845 cm^{-1}

are assigned to the stretching and bending vibrations of Mo=O in tetrahedrally coordinated molybdate (MoO_4^{2-}) and the 930 cm^{-1} band is due to the stretching vibrations of Mo=O in the octahedrally coordinated polymolybdate ($Mo_7O_{24}^{2-}$)[33]. As observed in the spectra of the CoMoE/BFA sample (Fig. 6e), the addition of EDTA induces a shift in the Mo=O stretching band to a higher wavenumber to 940 cm^{-1} with respect to the undistorted symmetry, which indicates that the supra-molecular structures were formed in the oxide catalysts, and it can be concluded that EDTA can modulate the interaction between the support and the active metals[33,34]. However, the fact that the band at about 940 cm^{-1} became stronger indicates that the addition of EDTA can lead to a formation of more polymolybdate species which are easy to be sulfided and transformed into more active phases in the presulfiding process. The peak at 990 cm^{-1} is attributed to the formation of the surface layer of MoO_3 aggregate[33] and it has been observed that the peak disappears in the spectra of the CoMoE/BFA sample, which implies that EDTA helps in the redispersion of these large octahedral MoO_3 crystallites. Besides, there are no obvious Raman bands for Co-O species, which suggests that Co is well dispersed in the Mo species. The high dispersion of active metals on the surface of support makes them easy to be sulfided in the presulfidation process, thus improve the catalytic activity.

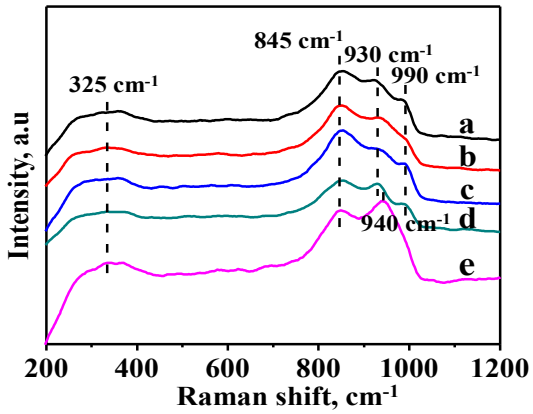

Fig. 6. Raman spectra of different catalysts. (a) CoMo/γ-Al_2O_3, (b) CoMo/FA, (c) CoMo/ZFA, (d) CoMo/BFA, (e) CoMoE/BFA

3.1.9 XPS analysis result

To analyze the sulfidation degrees of active metals on the surface of different supports, the fresh sulfide samples are characterized by XPS and the spectra are shown in Fig. 7. The analysis results obtained by the deconvolution method[35] are summarized in Table 3. The decompositions of the Mo3d spectra have been performed simulating each contribution with two peaks corresponding to the $Mo3d_{5/2}$ and $Mo3d_{3/2}$ core levels, and also the binding energy difference BE ($Mo3d_{5/2}$)-BE($Mo3d_{3/2}$) is equal to 3.15 eV, while the peak area ratio of $Mo3d_{5/2}/Mo3d_{3/2}$ is equal to 1.5 and the full width at half maximum (FWHM) of the $Mo3d_{5/2}$ and $Mo3d_{3/2}$ peaks are almost the same[36-38].

For the sulfided catalysts, the Mo3d spectra have been decomposed into the three well known contributions, which are attributed to Mo^{4+}, Mo^{5+} and Mo^{6+}, respectively. The Mo3d envelopes for the sulfided catalysts show strong doublets at the binding energies of 228.6±0.1 eV and 231.7±0.1 eV, which are the characteristics of $Mo^{4+}3d_{5/2}$ and $Mo^{4+}3d_{3/2}$, indicating the formation of MoS_2 species[39-42]. A relatively small peak at about 232.3 eV is assigned to Mo^{6+} species, indicating that a small fraction of Mo under oxidic form is still present after sulfidation. The presence of Mo^{5+} species of oxysulfide phases with weak peaks at 230.5 eV can also be observed. Therefore, the envelope of Mo3d is decomposed into Mo^{4+} and Mo^{6+} components as well as one peak at about 226.0 eV which is the characteristic of S2s.

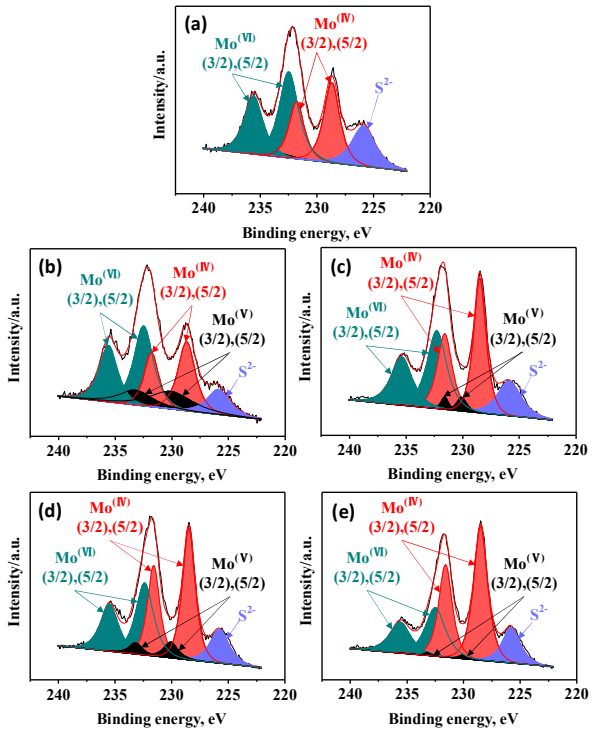

Fig. 7. Mo3d XPS spectra of different sulfided catalysts. (a) CoMo/γ-Al_2O_3, (b) CoMo/FA, (c) CoMo/ZFA, (d) CoMo/BFA, (e) CoMoE/BFA

Table 3. XPS characterization results of the series of MoCo sulfided catalysts. (A) CoMo/γ-Al_2O_3, (B) CoMo/FA, (C) CoMo/ZFA, (D) CoMo/BFA, (E) CoMoE/BFA

Catalysts	Mo^{4+}		Mo^{5+}		Mo^{6+}		S_M[b]
	ar.%[a] (228.9 eV)	ar.% (232.0 eV)	ar. % (230.5 eV)	ar. % (233.6 eV)	ar.% (232.5 eV)	ar.% (235.6 eV)	
A	21	14	12	8	27	18	35
B	25	17	3	2	32	21	42
C	30	20	3	2	27	18	50
D	32	21	4	3	24	16	53
E	35	23	1	1	24	16	58

Note: [a] ar. % means the area percent of XPS peak.
[b] $S_M = Mo_{sulfidation} = Mo^{4+}/(Mo^{4+}+Mo^{5+}+Mo^{6+})$.

It can be seen that the addition of EDTA does not change the binding energies of Mo species in the sulfided catalysts. The sulfidation degree of the Mo phase is assessed by using the fraction of Mo^{4+} species in the total Mo species. From the data in Table 3, it can be clearly seen that the $Mo_{sulfide}/Mo_{total} = Mo_{(IV)}/Mo_{total}$ increase

in the following order: CoMo/γ-Al_2O_3 < CoMo/FA < CoMo/ZFA < CoMo/BFA < CoMoE/BFA, which is in agreement with the active order. The XPS results demonstrate that Mo species over CoMoE/BFA catalyst are easy to be sulfided compared with other catalysts. Therefore, according to XPS analysis results, when the EDTA is used, Mo species can be dispersed and sulfided well, which is in consistent with the Raman results.

3.2 Catalytic performance evaluation

3.2.1. Catalytic performance in the hydro-upgrading of FCC gasoline

In this research, a series of catalysts of CoMo supported on different materials involving zeolite γ-Al_2O_3, FDU-12-γ-Al_2O_3, ZrFDU-12-γ-Al_2O_3 and BF-γ-Al_2O_3 were used to evaluate the catalytic performances for the hydro-upgrading of full-range FCC gasoline. The results were given in Table 4 and Fig. 8. CoMoE/BFA showed the highest HDS efficiency (94.2 %), and the lowest loss of octane number (0.8 unit). The highest i-paraffin (46.9 wt%) and aromatic (25.1 wt%) contents are the main reasons for its high preservation ability of RON. The best overall catalytic performance of CoMoE/BFA suggested that the addition of EDTA can significantly improve the activity of the catalysts.

Comparably, CoMo/BFA gave a relatively inferior catalytic performance, but was still higher than those of CoMo/γ-Al_2O_3, CoMo/FA and CoMo/ZFA. The catalytic performance of CoMo/BFA suggested that the incorporation of BF into the catalysts can improve the catalytic performances for HDS, hydroisomerization and aromatization.

Compared to CoMo/FA, the better HDS activity of CoMo/ZFA was assigned to Brønsted acidity, coming from the protons on the support surface resulting from the substitution of Si^{4+} by Zr^{3+} in the framework of FDU-12.

3.2.2. Effects of physicochemical properties of the catalysts on their catalytic performances

The catalytic performances of hydro-upgrading FCC gasoline over various catalysts are closely related to the physicochemical properties of the catalysts. Excellent textural properties largely contribute to the dispersion of active metals, mass transfer and stability.

In addition, acid property is also a crucial factor. Due to the L alkaline in nature of thiophene, the existence of L acid sites is conducive to the absorption and conversion of thiophene molecules. At the same time, B acid sites can facilitate C-S bond elimination and hydrogen transfer, which is very important for both hydrodesulfurization and isomerization reactions. The appropriate amount of L and B acid sites and their synergy are important for aromatization reactions. As shown in Table 2, the single γ-Al_2O_3-supported CoMo catalyst only contains plenty of L acid sites. Although isomerization of light paraffins is promoted by the weak and medium L acid sites over CoMo/γ-Al_2O_3, but hardly enough to preserve octane number[43]. However, the aromatization reaction can be enhanced through introducing B acid sites, so that the octane number of gasoline will be increased during the hydro-upgrading processes. There are two common ways to introduce B acid sites into the catalytic system. (1) As support additives , pure silicon FDU-12 material can be modified by heteroatoms such as (Al, Ti and Zr). (2) Another method is to add microporous zeolite into the support component. The synergy of two types of acid sites would produce a significant enhancement on hydro-isomerization and aromatization.

The addition of mesoporous silica FDU-12 improves the overall pore structure properties of the catalyst CoMo/FA, including the pore diameter and the specific surface area, which is conducive to enhancing the diffusion of sulfur-containing macromolecules contained in gasoline. However, the electronically neutral framework of pure silica FDU-12 leads to poor electronic effects of the acidity, which also restrains the proceedings of HDS, hydroisomerization and aromatization reactions[44].

The slight enhancements in the catalytic performances on CoMo/ZFA can be ascribed to the improvement of acidic properties by incorporating Zr species into FDU-12. CoMo/BFA possesses both the advantages of the excellent pore structure properties of mesoporous silica FDU-12 and the appropriate B and L acid properties of zeolite Beta. As support additive, micro/mesoporous composite material BF with large pore size and hierarchically porous structure has better anti-carbon deposition ability as well as larger pore structure to enhance the diffusion of macromolecules. High specific surface area favors the dispersion of active metals, which facilitates the contacts with the reactant molecules. Moreover, appropriate amounts of B and L acid sites with moderate acid strength achieve a good balance among the HDS, hydroisomerization and aromatization reactions[45].

Table 4. Hydrotreatment results of FCC gasoline over different catalysts. (A) CoMo/γ-Al_2O_3, (B) CoMo/FA, (C) CoMo/ZFA, (D) CoMo/BFA, (E) CoMoE/BFA

Catalyst	Feed	A	B	C	D	E
PONA/m%	-	-	-	-	-	-
n-Paraffin	6.6	13.2	13.1	11.1	10.7	9.4
i-Paraffin	33.7	43.8	44.0	44.5	45.4	46.9
Olefin	29.5	8.7	8.5	8.6	9.3	8.8
Naphthene	8.0	10..8	11.0	11.8	10.2	9.8
Aromatics	22.2	23.5	23.4	23.9	24.4	25.1
Sulfur, mg/L	660	111	107	96	51	38
HDS%	-	83.2	83.8	85.5	92.2	94.2
RON	91.3	89.7	89.6	90.1	90.2	90.5
△RON	-	-1.6	-1.7	-1.2	-1.1	-0.8

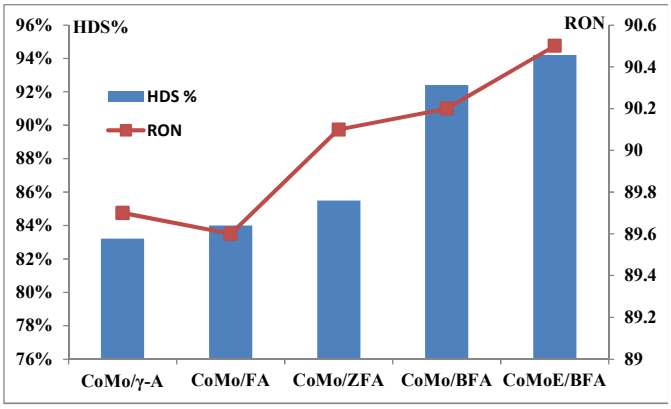

Fig. 8. Hydrotreatment results of FCC gasoline over different catalysts.

The addition of EDTA improves the dispersion of the active metals by the post-treatment method based on the characterization results of XRD, UV-vis and Raman analysis, furthermore, moderates the interactions between the metals and the supports by forming the supramolecular structures[34]. It could be also observed from XRD characterization results that the CoMo/BFA prepared without chelating agents shows the presence of the β-$CoMoO_4$ crystalline phase. Chelating agents prevent the formation of this crystalline phase which is unfavorable to HDS reaction. In addition, from the characterization results of XPS, the EDTA modified catalyst has a higher degree of sulfidation due to the better dispersion of the active metals, which is conductive to improve the hydro-upgrading performance. Thus, CoMoE/BFA achieves a much better result, i.e., HDS efficiency 94.2% and RON loss 0.8 unit.

4. Conclusions

In this study, a novel kind of micro/mesoporous composite material Beta-FDU-12 (BF) was successfully synthesized via a nano-assembling method. The characterization results showed that BF composite possessed the Fm3m cubic ordered mesoporous structure similar to the pure silica material FDU-12, and its framework simultaneously contained the microporous structure of Beta zeolite. The textural and acidity properties of the BF composite were improved compared with those of zeolite Beta and mesoporous FDU-12, and the corresponding catalyst CoMo/BFA also showed a high HDS activity (92.2 %) and low RON loss (1.1 units).

Furthermore, the EDTA modified catalyst CoMoE/BFA exhibited a good balance in HDS, hydroisomerization and aromatization activities, giving the highest HDS efficiency (94.2 %) and the lowest RON loss (0.8 unit). As a result, the presence of Brønsted acidic sites, desirable textural properties, and better dispersion results in a comparable HDS activity of CoMoE/BFA than other reference catalysts.

Acknowledgement

This work was supported by National Natural Science Foundation of China (No. 21276277 and U1463207), CNOOC project and CNPC major project.

Notes and References

1 Z. Liu, L. Zhang, J. Jiang, et al. Adv. Chem. Eng. Sci., 2013, **03**, 36-46.
2 A. Olivas, T.A. Zepeda. Catal. Today, 2009, **143**, 120-125.
3 J.N. Díaz de León, M. Picquart, L. Massin, et al. J. Mole. Catal. A, 2012, **363-364**, 311-321.
4 T. Klimova, J. Reyes, O. Gutiérrez, et al. Appl. Catal. A, 2008, **335**, 159-171.
5 A. Infantes-Molina, J.A. Cecilia, B. Pawelec, et al. Appl. Catal. A, 2010, **390**, 253-263.
6 P.E. Boahene, K.K. Soni, A.K. Dalai, et al. Appl. Catal. A, 2011, **402**, 31-40.
7 A. Corma, V. Fornés, J.B. Montón, et al. J. Catal., 1987, **107**, 288-295.
8 M.A. Ali, T. Tatsumi, Appl. Catal. A, 2002, **233**, 77-90.
9 D.L. Fletcher, T.L. Hilbert, S.J. Mcgovern et al. Gasoline Upgrading Process: US, Pat. 5413696. 1995.
10 D.L. Fletcher, M.N. Harandi, M.S. Sarli et al. Hydrocarbon Upgrading Process: US, Pat. 5413698. 1995.
11 B. Chawla, D.N. Mazzone, M.S. Sarli et al. Gasoline Upgrading Process: US, Pat. 5411658. 1995.
12 J. Fan, C. Yu, F. Gao, Angew. Chem. Int. Ed., 2003, **115**, 3254-3258.
13 P. Salas, J.A. Wang, H. Armendariz, et al. Mater. Chem. Phys., 2009, **114**, 139-144.
14 O.Y. Gutiérrez, G.A. Fuentes, C. Salcedo, et al. Catal. Today, 2006, **116**, 485-497.
15 O.Y. Gutiérrez, F. Pérez, G.A. Fuentes, et al. Catal. Today, 2008, **130**, 292-301.
16 D. Valencia, T. Klimova. Catal. Today, 2011, **166**, 91-101.
17 Y. Liu, W. Zhang, T.J. Pinnavaia. J. Am. Chem. Soc., 2000, **122**, 8791-8792.
18 H. Wu, A. Duan, Z. Zhao, et al. J. Catal., 2014, **317**, 303-317.
19 D. Zhang, A. Duan, Z. Zhen, et al. J. Catal., 2010, **274**, 273-286.
20 S. Badoga, A.K. Dalai, J. Adjaye, et al. Ind. Eng. Chem. Res., 2014, **53**, 2137-2156.
21 H. Wu, A. Duan, Z. Zhao, et al. Fuel, 2014, **130**, 203-210.
22 R. Cattaneo, T. Shido, R. Prins. J. Catal., 1999, **185**, 199-212.
23 S, Badoga, K.C. Mouli, K. Soni, et al. Appl. Catal. B, 2012, **125**, 67-84.
24 L. Pena, D. Valencia, T. Klimova. Appl. Catal. B, 2014, **147**, 879-887.
25 J. Fan, C. Yu, J. Lei, et al. J. Am. Chem. Soc., 2005, **127**, 10794-10795.
26 Q.J. Yu, C. Li, L. Xu et al., Chin. J. Catal., 2001, **22**, 469-474.
27 P. Prokešová, S. Mintova, J. Čejka, et al. Micropor. Mesopor. Mater., 2003, **64**, 165-174.
28 X. Bao, X. Zhao. J. Phys. Chem. B, 2005, **109**, 10727-10736.
29 J. Perez-Pariente, J.A. Martens, P.A. Jacobs. Appl. Catal., 1987, **31**, 35-64.
30 R. Huirache-Acuña, T.A. Zepeda, E.M. Rivera-Muñoz, et al. Fuel, 2014, **149**, 149-161.
31 R.S. Weber. J. Catal., 1995, **151**, 470-474.
32 J. RamíRez, R. Contreras, P. Castillo, et al. Appl. Catal. A, 2000, **197**, 69-78.
33 P.V. La, G. Deganello, C.R. Tewell, et al. Appl. Catal. A, 2002, **235**, 171-180.
34 D. Valencia, L. Peña, V.H. Uc, et al. Appl. Catal. A, 2014, **475**, 134-139.

35 L. Qiu, G. Xu, Appl. Surf. Sci., 2010, **256**, 3413-3417.
36 P. Beccat, P.D. Silva, Y. Huiban et al., Oil Gas Sci. Tech. Rev. 1999, **487**, 54.
37 N. Frizia, P. Blanchard, E. Payen, Catal. Today, 2008, **130**, 272-282.
38 L. Benoist, D. Gonbeau, G. Pfister-Guillouzo et al., Thin Solid Films, 1995, **258**, 110-114,
39 F. Takashi, K. Masahiro, E. Takeshi, J. Jpn. Petrol. Inst. 2005, **48**, 114.
40 J.C. Muijsers, T. Weber, R.M. Hardeveld, J. Catal. 1995, **157**, 698-705.
41 A.F.H. Sanders, A.M.D Jong, V.H.J. Beer, Appl. Surf. Sci. 1999, **144**, 380-384.
42 J.E. Herrera, D.E. Resasco, J. Catal. 2004, **221**, 354-364.
43 Y. Fan, D. Lei, G. Shi, et al. Catal. Today, 2006, **114**, 388-396.
44 D. Solís, A.L. Agudo, J. Ramírez, et al. Catal. Today, 2006, **116**, 469-477.
45 P. Rayo, J. Ramírez, P. Torres-Mancera, et al. Fuel, 2012, **100**, 34-42.

GRAPHICAL ABSTRACT

Micro/mesoporous composite material Beta-FDU-12 was successfully synthesized by a nano-assembling method. The composite material was used as the support additive and the corresponding catalyst CoMo/BFA was evaluated in the hydro-upgrading of FCC gasoline. Furthermore, EDTA was added by the post-treatment method to improve active metals dispersity on the catalyst CoMo/BFA and to moderate the interaction between the active metal and support. The catalyst CoMoE/BFA exhibited better hydro-upgrading performance of FCC gasoline (HDS efficiency 94.2 % and RON loss 0.8 unit).